ChemCatChem

Research Article
doi.org/10.1002/cctc.202400711

Chemistry Europe
European Chemical Societies Publishing

www.chemcatchem.org

How Can the Diterpene Synthase CotB2^{V80L} Alter the Product Profile?

Stephanie Himpich[+],[a] Marion Ringel[+],[b] Renana Schwartz[+],[c] Nicole Dimos,[a] Ronja Driller,[a] Carl P. O. Helmer,[a] Prashant Kumar Gupta,[c] Martina Haack,[b] Dan Thomas Major,*[c] Thomas Brück,*[b] and Bernhard Loll*[a]

Structural diversity of diterpenes is mediated by the enigmatic family of diterpene synthases. The overall enzymatic contribution hereby lies in a carefully concerted chemistry of highly reactive carbocation intermediates mainly guided by aromatic and polar amino acid side chains and the pyrophosphate cofactor. To date several studies aimed to shed light on the mechanism underlining terpene synthases chemistry. Specifically, the diterpene synthase CotB2 serves as model enzyme for detailed mutagenesis studies. Here we investigate the catalytic mechanism of CotB2 variant V80L in a holistic, biochemical, structural, and computational biology approach. We were able to identify an altered product profile compared to CotB2^{WT} for the substrates geranylgeranyl diphosphate and farnesyl diphosphate. Moreover, we solved the crystal structure, and shed further light on terpene synthase chemistry by modelling of the substrate and intermediate binding.

Introduction

Terpenes represent one of the most diverse and structurally complex class of biomolecules generated by nature.[1–5] Miscellaneous bioactivities arise from this vast diversity of natural products that are of profound industrial interest. In contrast to chemical synthesis of terpenes, terpene synthases (TPSs) offer a sustainable route to produce these bioactive molecules at an industrially relevant scale using biotechnology principles.

A well-established TPS model is the terpene cyclase CotB2, a bacterial diterpene synthase derived from the cyclooctatin biosynthetic gene cluster of *Streptomyces melanosporofaciens*. Cyclooctatin shows potent anti-inflammatory activity, thus the elucidation and control of cyclooctatin biosynthesis is of high interest for the pharmaceutical sector. CotB2 is responsible for the synthesis of the intermediate cyclooctat-9-en-7-ol.[6] It catalyses the cyclization of the linear, aliphatic substrate *E*,*E*,*E*-geranylgeranyl diphosphate (GGDP), and represents the first committed step in the biosynthesis of cyclooctatin. Initially, it was reported that the only substrate of CotB2 is GGDP.[6] Recently, it was demonstrated that CotB2 can also cyclize farnesyl diphosphate (FDP) as an alternative substrate.[7] In addition to the cyclization activity, a prenylation activity was detected for CotB2, with indole as a substrate in presence of dimethylallyl diphosphate or geranyl diphosphate.[8]

CotB2 has been identified to perform a highly specific regio- and stereochemical reaction. Further, several mutagenesis studies revealed, that this highly specific biosynthesis cascade can be reprogrammed by single amino acid substitutions, with a focus on aromatic amino acid side chains in the active site generating alternative diterpene products with diverse bioactivities.[9–11] Further structural and biochemical characterization and structure-based mutagenesis approaches, can pave the way for new drug lead alternatives to cyclooctatin.[9–12]

CotB2 belongs to class I TPSs, that initially generate an allylic carbocation by the release of pyrophosphate in a trinuclear Mg^{2+}-metal cluster. The members of this class comprise two distinct motifs, an aspartate-rich DDXXD motif binding the diphosphate group of the substrate and a NSE/DTE motif, which supports correct positioning of the substrate with a trinuclear Mg^{2+} cluster. Upon binding of the substrate and three Mg^{2+} cations, TPSs undergo a conformational change from an open to a closed conformation. Biochemical, and structural investigations of CotB2 and variants, revealed the importance of the last 13 C-terminal amino acids. Upon closure of the active site, this initially unstructured loop forms a lid over the active site.[11] Thereby a C-terminal RY-pair establishes interaction with the substrate and the aspartate-rich as well as the NSE motif. This closed conformation was shown to be a prerequisite for enzymatic activity, underlined by the fact, that the CotB2 variant terminating at R294 lacking the last 12 C-terminal residues (CotB2$^{\Delta C}$) is an inactive variant, defective in binding the substrate, hence not capable of catalysis.[11] Even

[a] S. Himpich,[+] N. Dimos, R. Driller, C. P. O. Helmer, B. Loll
Freie Universität Berlin, Institut für Chemie und Biochemie, Strukturbiochemie, Takustr. 6, 14195 Berlin, Germany
E-mail: loll@chemie.fu-berlin.de

[b] M. Ringel,[+] M. Haack, T. Brück
Department of Chemistry, Technical University of Munich (TUM), Werner Siemens Chair of Biotechnology, TUM School of Natural Sciences, Lichtenbergstr. 4, 85748 Garching, Germany
E-mail: brueck@tum.de

[c] R. Schwartz,[+] P. Kumar Gupta, D. Thomas Major
Department of Chemistry, Department of Chemistry, Bar-Ilan University, Ramat-Gan 52900, Israel
E-mail: Dan-Thomas.Major@biu.ac.il

[+] Authors contributed equally.

Supporting information for this article is available on the WWW under https://doi.org/10.1002/cctc.202400711.

though two Mg^{2+} cations were bound to the structure, we failed to crystallize CotB2$^{\Delta C}$ in its closed conformation in line with the observation that no product formation was detected in our *in vivo* production system.[11] For the variant CotB2^{V80L} we could previously not detect activity in our *in vivo* production system. Therefore, we assumed that CotB2^{V80L} is not capable to transit from the open, to the closed conformation. Hence, we questioned the reason of inactivity, which could be caused by a decreased stability of the CotB2 variant and/or by the larger side chain at position 80, which could potentially interfere with the cyclization reaction. To gain a more detailed molecular understanding of the inactivity of CotB2^{V80L}, we performed differential scanning fluorometry (DSF) and crystallization experiments to obtain structural information of the variant. Since the bulkier side chain at position 80, is expected to reduce the volume of the mainly hydrophobic active site, we further tested the activity of CotB2^{V80L} in an *in vitro* setup with recombinantly produced CotB2^{V80L} towards the smaller substrate FDP and the natural substrate GGDP. Subsequently the products were analysed by GC/MS. Our biochemical and biophysical experiments are supplemented with EnzyDock quantum mechanics/molecular mechanics (QM/MM) docking to gain deeper insights in the cyclization mechanism of this highly interesting CotB2 variant. To our knowledge this is the first study focusing on the role of a non-aromatic amino acid in the CotB2 active site vicinity showing a significant effect on catalysis, substrate selectivity and specificity of the product profiles.

Results and Discussion

Biochemical Characterization

We expressed CotB2^{V80L} in *Escherichia coli* and purified CotB2^{V80L} to high purity (Figure S1). To test whether the single amino acid exchange could potentially have an effect on protein stability, we performed DSF. We determined the melting temperature (T_M) of CotB2^{V80L} in comparison to CotB2^{WT} as well as the T_M of both proteins, each incubated with 4-amino-1-hydroxy-1-phosphonobutyl-phosphonate (alendronate (AHD)), a compound that mimics the diphosphate group of GGDP generating the closed conformation. CotB2^{WT} in its open conformation has a T_M of 43.6 °C and upon transition to the closed conformation the T_M is increased to 56.9 °C (Figure S2). The inactive CotB2$^{\Delta C}$ variant is not stabilized by AHD with an essentially unchanged T_M (Figure S2c), indicating that AHD cannot bind to CotB2$^{\Delta C}$. CotB2^{WT} as well as the variant CotB2^{V80L} have an identical T_M for the open conformation (Figure S2), demonstrating that the single mutation has no influence on the overall stability of CotB2^{V80L}. Upon addition of AHD the T_M of CotB2^{V80L} increased by 16.0 °C, indicating that CotB2^{V80L} can undergo the transformation from the open to the closed conformation (Figure S2a and b). The observation of a conformational change from the open to the closed conformation is indicative of a putative enzymatic activity of CotB2^{V80L}. To test this hypothesis on a molecular level, we subsequently initiated a structural characterization of CotB2^{V80L}.

Structural Characterization

The overall structure of CotB2^{V80L} in its open conformation was determined to 1.6 Å resolution (Table S1). The structure is essentially identical to CotB2^{WT} (PDB-ID 4OMG;[11]). Both structures superimpose with a root mean square deviation (rmsd) of 0.2 Å for 258 pairs of Cα atoms. The side chain of L80 points towards the hydrophobic reaction chamber (Figure S2a). Changes are restricted to the local environment of the altered amino acid. As expected for the open conformation, the last 16 C-terminal amino acids are flexible with a lack of interpretable electron density.

Structure of CotB2$^{V80L}\cdot Mg^{2+}{}_3\cdot$AHD

To generate the closed conformation, we co-crystallised CotB2^{V80L} with AHD (Figure S3b). The structure of CotB2$^{V80L}\cdot Mg^{2+}{}_3\cdot$AHD was solved to 1.6 Å resolution (Table S1) and adopting the same overall structure and active site architecture as described for CotB2$^{WT}\cdot Mg^{2+}{}_3\cdot$AHD (PDB-ID 6GGJ;[11] with a rmsd of 0.3 Å for 260 pairs of Cα atoms (Figure 1a). The N-terminal portion of α-helix C is shifted outwards of the active site (Figure 1a). Compared to CotB2^{WT} the α-helix C is tilted by 3° (angle between the Cα-atoms of CotB2$^{WT/R73}$, CotB2$^{V80L/Q85}$, and CotB2$^{V80L/R73}$), leading to a rmsd of 0.4 Å for 12 pairs of Cα atoms (CotB2 $^{V80/R73}$ CotB2 $^{V80/R73}$). The catalytic motifs of CotB2$^{V80L}\cdot Mg^{2+}{}_3\cdot$AHD (Figure S4) are arranged as described before for the closed conformation of CotB2^{WT} and its variants.[11] The closed conformation is accompanied with its C-terminus folding over the active site to shield it from bulk solvent.[11–12] Closure leads to a formation of a salt-bridge between D111 of the aspartate-rich motif and R294

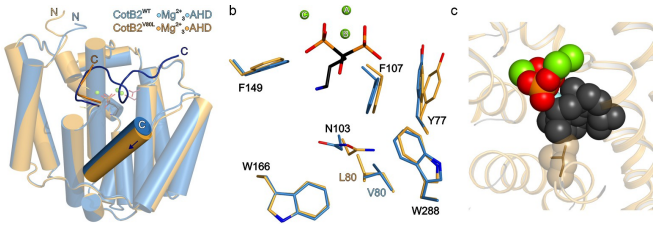

Figure 1. (a) Superposition of the closed conformation of CotB2$^{WT}\cdot Mg^{2+}{}_3\cdot$AHD (PDB-ID 6GGJ,[11] coloured in light blue, and CotB2$^{V80L}\cdot Mg^{2+}{}_3\cdot$AHD, coloured in light orange. Highlighted is α-helix C, which due the mutation at position 80 tilts away from the active site. (b) View into the active site of CotB2$^{WT}\cdot Mg^{2+}{}_3\cdot$AHD superimposed on the structure of CotB2$^{V80L}\cdot Mg^{2+}{}_3\cdot$AHD. Notably, Y77 occurs in a double conformation with an impact on the conformation of the C-terminus. (c) Structure of the closed conformation of CotB2$^{V80L}\cdot Mg^{2+}{}_3\cdot$AHD with the Mg^{2+} and AHD omitted. In space-filling representation, the diphosphate moiety (oxygen in red and phosphorous in orange) with bound Mg^{2+} cations (green spheres) and 2-fluoro-3,7,18-dolabellatriene (F-Dola; black for carbon atoms and light blue for fluorine), as obtained by superposition with the structure of CotB2$^{WT}\cdot Mg^{2+}{}_3\cdot$F-Dola (PDB-ID 6GGI[11]).

(Figure S4). Moreover, Y295 establishes hydrogen bonds to the phosphate function of AHD as well as to N220 of the NSE motif.

A closer inspection of the active site reveals, that the V80 L exchange has no major influence on the side chain conformation of previously reported residues,[9,11–13] such as F107, F149, and W288, all crucial for the propagation of the carbocation (Figure 1b).

The larger volume of the active site allows the side chain of Y177 to adopt a double conformation (Figure 1b), not observed in any of the reported CotB2 variants or CotB2^{WT} structures in their closed conformation. Notably, one of the side chain conformations of Y177, resembles a side chain conformation in the open conformation of CotB2^{V80L}. Further, residues of α-helix C are in contact with the C-terminal portion, termed the lid region, of CotB2. In the structure of CotB2^{V80L}·$Mg^{2+}{}_3$·AHD, in comparison to CotB2^{WT} or other variant structures of CotB2, we could only partially model the C-terminus (Figure 1a).

Next, we superimposed the structure of CotB2^{WT} bound to three Mg^{2+} cations, a diphosphate moiety and 2-fluoro-3,7,18-dolabellatriene (CotB2^{WT}·$Mg^{2+}{}_3$·F-Dola; PDB-ID 6GGI;[11]) with the structure of CotB2^{V80L}·$Mg^{2+}{}_3$·AHD. The superposition clearly demonstrates, that the bulkier leucine residue would sterically interfere with a bound product, thereby interfering with the cyclization cascade (Figure 1c). To this end, the closest distance between the side chain carbon atom CD2 of L80 and the carbon atom CNN of F–Dola is 2.2 Å. In contrast the closest carbon-carbon distance between V80 and F-Dola is 3.6 Å. Hence the structure of CotB2^{V80L}·$Mg^{2+}{}_3$·AHD demonstrates, that the single amino acid exchange has no impact on the transition from the open to the closed conformation. Given the enigmatic observation of the closing ability of CotB2^{V80L}, we further investigated the product formation of this variant in context of the altered active site cleft.

Cyclization Activity with Geranylgeranyl Diphosphate

Initial screens on product formation of CotB2^{V80L} revealed a substantially altered product portfolio compared to CotB2^{WT}.[11] We therefore tested CotB2^{V80L} alongside with CotB2^{WT} in our *in vitro* assay system for their ability to cyclize GGDP in order to get detailed insights into the product profile. Subsequent gas chromatography evaluation of the products revealed diterpenoid products with a prominent peak at RT accounting for 3,7,18-dolabellatriene when compared to reference spectra (Figure 2a and S5, S6). Further products of CotB2^{V80L} with the substrate GGDP are cyclooctat-1,7-diene, 3,7,12-dolabellatriene, two dolabellane-type diterpenes as well as minor amounts of the WT main product cyclooctat-9-en-7-ol (Figure 2c and S8). Our novel findings are in contrast to our initially detected inactivity of CotB2^{V80L} in our *in vivo* production pipeline.

Cyclization Activity with Farnesyl Diphosphate

We questioned whether a smaller substrate, such as FDP could be cyclized by CotB2^{V80L}, which has been described for CotB2^{WT}

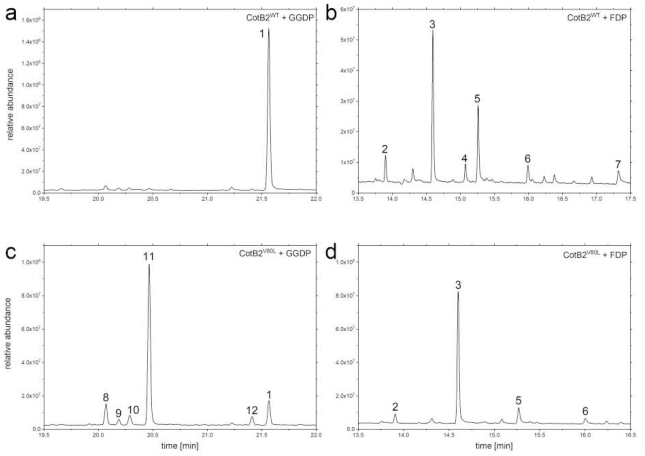

Figure 2. GC–MS analysis of the product spectrum of CotB2^{WT} and CotB2^{V80L} with the substrates GGDP and FDP, respectively. Numbers of compounds refer to Figure S5. Product distribution in percentage is shown in Table S3. (a) Product profile of CotB2^{WT} with GGDP as substrate. Main product cyclooctat-9-en-7-ol, **1** (RT = 21.57 min). (b) Product profile of CotB2^{WT} with FDP as substrate: β-elemene, **2** (RT = 13.91 min), β-farnesene, **3** (RT = 14.60 min), farnesene sesquiterpene, **4** (RT = 15.08 min), α-farnesene, **5** (RT = 15.27 min), nerolidol, **6** (RT = 16.00 min), α-farnesol, **7** (RT = 17.33 min). (c) Product profile of CotB2^{V80L} with GGDP as substrate: cyclooctat-1,7-diene, **8** (RT = 20.07 min), 3,7,12-dolabellatriene, **9** (RT = 20.19 min), dolabellane-type diterpene, **10** (RT = 20.19 min), 3,7,18-dolabellatriene, **11** (RT = 20.47 min), dolabellane-type diterpene, **12** (RT = 21.41 min), cyclooctat-9-en-7-ol, **1** (RT = 21.57 min). (d) Product profile of CotB2^{V80L} with FDP as substrate: β-elemene, **2** (RT = 13.91 min), β-farnesene, **3** (RT = 14.60 min), α-farnesene, **5** (RT = 15.27 min), nerolidol, **6** (RT = 16.00 min). High resolution mass spectra of compounds **4**, **10**, and **12** are shown in Figure S15–S17.

previously.[7] We subsequently tested CotB2^{WT} and CotB2^{V80L} in our *in vitro* systems for their ability to cyclize FDP. Interestingly, both were active towards FDP, producing a variety of sesquiterpenes (e.g., β-elemene, β-farnesene, α-farnesene, nerolidol) (Figure 2b, d S7 and S9). To this end, CotB2^{WT} and CotB2^{V80L} generated almost identical product spectra. However, in our experiment CotB2^{V80L} generated a more specific product spectrum compared to CotB2^{WT}, despite the larger active site volume.

Computational Studies of CotB2^{V80L}

To gain an atomic level understanding of the substrate folding mechanism of the CotB2^{V80L} variant, we performed molecular docking simulations of GGDP in WT and variant enzymes. The complete reaction mechanism for the formation of cyclooctat-9-en-7-ol from GGDP in CotB2^{WT} has been discussed in detail in our previous work.[12] Here, we discuss the initial stages of the reaction mechanism, which forms carbocation **A** (Scheme 1).

Docking in CotB2^{WT} and CotB2^{V80L}

The CotB2^{WT} crystal structure (PDB-ID 6GGI) of the holo-enzyme contains the deprotonated fluorinated product of cation A (Figure 3a). The correctly folded state of GGDP in the hydro-

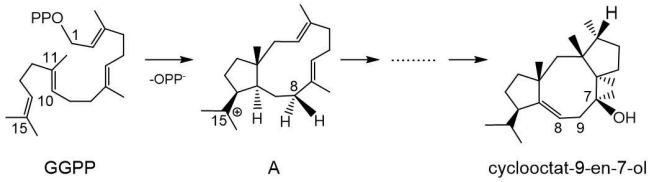

Scheme 1. Reaction mechanism in CotB2^{WT}. Only GGDP, the intermediate dolabellatrienyl cation (A) and the final product are shown.

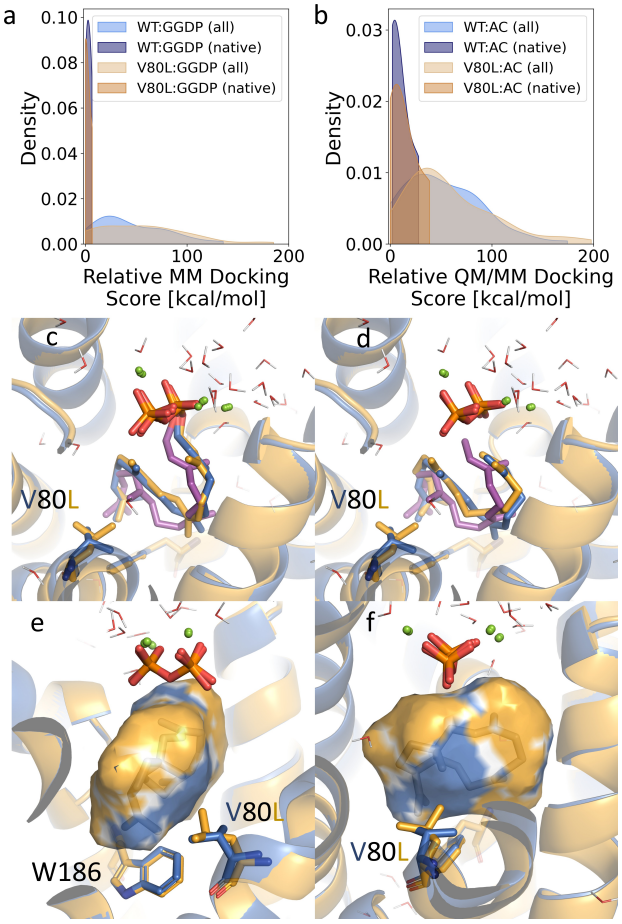

Figure 3. Relative docking score density for CotB2WT and CotB2 V80 L for (a) GGDP using MM and (b) for the initial allyl cation (AC) using QM(HF3c)/MM. Docked poses in CotB2WT and CotB2 V80 L for (c) GGDP using MM and (d) for the initial AC using QM(HF3c)/MM compared to GGDP docked in [11]. Shown in (e) and (f) are the binding site excess volumes in CotB2WT and CotB2 V80 L, in complementary orientations. Light blue color shows excess volume in CotB2WT, while light orange color shows excess volume in CotB2V80L.

phobic pocket of CotB2^{WT} has been validated in our previous work based on multistate EnzyDock simulations and QM/MM free energy calculations.[11–12] and is used as the reference structure in this work.

The correctly folded GGDP is such that following initial heterolytic cleavage of the substrate C–O bond, concerted bond formations between C1-C11 and C10-C14 lead to formation of cation **A** (Scheme 1). This correctly folded state of GGDP requires the pairs C1-C11 and C10-C14 atoms to be in close proximity (Figure 3c, d). Additionally, the orientation of the methyl group at C11 must allow C1 to attack the *si*-face of C11. Careful inspection of the docking energies (Figure 3a, b) and preferred docked poses in CotB2^{WT} and CotB2^{V80L} shows that GGDP folds correctly in both enzymes (Figure 3c, d). EnzyDock docking using both MM and QM/MM scoring shows that the correct, native substrate fold is in the low-energy region of the energy space (Figure 3a, b). Hence, presumably, both WT and the V80 L variant can form intermediate carbocation **A**, although this carbocation is quenched in the variant enzyme. This premature quenching may be explained by inspection of the active site volume in the two enzyme forms. The computed volume in CotB2^{WT} is 312 ± 1 Å^3 and 321 ± 1 Å^3 in CotB2^{V80L}. This larger volume in the mutant enzyme is due to a shift in helix C as observed in the crystal structure. We generated an AlphaFold2[14] model for CotB2^{V80L} and the model does not show the helical shift, underscoring the need for a crystal structure. We also computed the excess volume in CotB2^{WT} and CotB2^{V80L} relative to the joint volume of the two enzymes (i.e., the intersection of the two volumes). In Figure 3e, f the excess volume in CotB2^{WT} is coloured in light blue, while in CotB2^{V80L} it is coloured light orange. As expected, in the vicinity of the mutation, there is excess volume in CotB2^{WT}. However, due to the overall enlarged volume in CotB2^{V80L} there is more room for intermediate **A**, which has a smaller effective volume than the substrate GGDP, to wiggle. We proposed, that this allows penetration of one or more water molecules in the vicinity of the cation at C15, which could facilitate premature deprotonation to form dolabellatriene. We note, that the electrostatic potentials in the active site in the two enzyme forms are similar (Figure S10).

Free MD-Simulation

To further investigate the water content of the binding pocket, all-atom, room-temperature MD simulations of CotB2^{WT} and CotB2^{V80L} were performed with 3 replicas of 10 ns. The water density was analyzed and revealed specific regions in space where water molecules were consistently present during the simulations. Three main positions were found that may interact with the ligand (Table S2). W1 is a conserved water position as revealed in previous work and binds N220 (ND2), N285 (OD1, ND2) and T289 (OG1).[11] The density at this site was slightly broader in the CotB2^{V80L} simulations than in the CotB2^{WT} simulations, hinting at increased flexibility and likelihood of getting closer to the ligand at an early stage of the mechanism and quench the reaction (Figures S11–S12). W2 is an auxiliary site to that also binds N285 (OD1 or ND2) and hence may assist in a proton-transfer chain. It also binds I282 (O), G215 (O) and appear in the crystal structures. A significant density was found for this site in three CotB2^{V80L} simulations and one CotB2^{WT} simulation, which might assist in the process of pre-mature quenching. W3 is close to a proposed catalytic position,[11–12] where a water is bound to N103 (O and OD1), and T106 (OG1). The position is ~3.5 Å away from W581 (PDB ID: 7AO3[12]). Occupation of this site was observed in two CotB2^{V80L}

simulations. In conclusion, we observe additional water sites in the CotB2^{V80L} simulations compared to the CotB2^{WT} simulations, and we ascribe this to the larger volume in the former.

Conclusions

In the past, single amino acid exchanges of residues have been performed.[10–11,15] Since aromatic side chains are involved in propagation and stabilization of the highly active carbocations, those amino acid side chains have been the prime target. One exception is N103, due its potential role in the final quenching leading to the hydroxylation to the final cyclization product cyclooctat-9-en-7-ol. We have reinvestigated the variant CotB2^{V80L}, which had previously been described as an inactive variant.[11] We determined the structure of CotB2^{V80L} in its open and closed conformation. The structures agree with the observation of the DSF that CotB2^{V80L} is stabilized upon binding of AHD and can adopt the closed conformation. Our *in vitro* studies with purified CotB2^{V80L} and the substrate show an altered product profile compared to CotB2^{WT}. This might be caused by the substitution of valine at position 80 by leucine, which leads to a shift in helix C. As a consequence, the volume of the active site is increased, and there is more room for intermediate **A**, which has a smaller effective volume than the substrate f, to wiggle. Based on EnzyDock docking and MD simulations, we proposed that this allows penetration of one or more water molecules in the vicinity of the cation at C15, which could facilitate premature deprotonation to form dolabellatriene. A superposition of the structures of CotB2$^{V80L}\cdot Mg^{2+}{}_3\cdot$AHD and of CotB2$^{WT}\cdot Mg^{2+}{}_3\cdot$F-Dola reveals that the distance between the substrate intermediate analogue F-Dola and residue L80 is potentially too small. This observation raised the question, whether CotB2^{V80L} could cyclize the smaller isoprene-unit FDP. Interestingly, the products of the cyclization reaction with FDP are identical to CotB2^{WT}.[7] Hence the reaction with FDP is not affected by the mutation of valine to leucine. Our finding encourages not to restrict amino acid exchanges to aromatic amino acid side chains.

Experimental Section

Protein Expression and Purification

Cloning of the CotB2^{V80L} construct has been described in ref. [11]. CotB2^{V80L} fused to a C-terminal hexa-histidine-tag in a pET-24a vector were expressed in *E. coli* Rosetta2 DE3 cells.[11] Cells were harvested by centrifugation (6 min, 6,000 rev min^{-1} at 4 °C) and resuspended in buffer A (50 mM Tris/HCl pH 7.5, 500 mM NaCl, 5 mM $MgCl_2$, 1 mM DTT). The cells were lysed by homogenisation and the lysate was cleared by centrifugation (1 h, 21,000 rev min^{-1} at 4 °C). Purification included Ni^{2+}–NTA affinity chromatography (elution in a linear gradient to buffer A containing 500 mM imidazole) and subsequent size-exclusion chromatography in buffer B (20 mM Tris/HCl pH 7.5, 150 mM NaCl, 5 mM $MgCl_2$, 1 mM DTT).[9,15]

Crystallisation

CotB2^{V80L} was concentrated to 28 mg/ml as measured by the absorbance at 280 nm. Crystals were obtained by the sitting-drop vapour-diffusion method at 18 °C with a reservoir solution composed of 19% (w/v) polyethylene glycol 8000 and 0.1 M CAPS at pH 10.0. For co-crystallization experiments with alendronate (Alfa Aesar, Germany), CotB2^{V80L} was incubated in a 2-fold molar excess for 30 min on ice. Crystals were obtained by the sitting-drop vapor-diffusion method at 18 °C with a reservoir solution composed of 7% (w/v) polyethylene glycol 8,000, 0.15 M $Mg(CH_3COO)_2$ and 10% (v/v) ethylene glycol. All crystals were cryo-protected with 25% (v/v) 2-methyl-2,4-pentanediol supplemented to the reservoir resolution and subsequently flash-cooled in liquid nitrogen.

Structure Determination and Refinement

Synchrotron diffraction data were collected at the beamline 14.2 of the MX Joint Berlin laboratory at BESSY (Berlin, Germany) and beamline P14 or beamline P11 of PETRA III (Deutsches Elektronen Synchrotron, Hamburg, Germany) at 100 K Diffraction data were processed with XDS[16] (Table S1). The structures were determined by molecular replacement with the coordinates of CotB2^{wt} (PDB-ID: 4OMG[9]) as search model using PHASER.[17] The structures were refined by maximum-likelihood restrained refinement in PHENIX[18] Model building and water picking was performed with COOT. Model qualities were evaluated with MolProbity[19] and the JCSG validation server (JCSG Quality Control Check v3.1). Figures were prepared using PyMOL (Schrodinger Inc).

Differential Scanning Fluorometry (DSF)

Melting temperatures of CotB2^{WT}, CotB2^{V80L}, and CotB2$^{\Delta C}$ were measured with the Mx3005P qPCR system (Agilent) in a 96-well plate format with and without alendronate. Each well contained 8 μl buffer B, 10 μl protein (0.15 μg/μl) with 10x SYPRO Orange dye (Invitrogen) end concentration and either 2 μl water or 2 μl alendronate (0.6 mg/ml). The program consisted of three steps: step 1 was a pre-incubation for 1 min at 20 °C, and steps 2 and 3 were cycles comprising the temperature increase of 1 °C within 20 s. The temperature gradient proceeded from 25 to 95 °C at 1 °C per minute. Samples were measured in triplicates. The data was acquired with MxPro QPCR software (Agilent) and analysed with DSF Analysis v3.0.1 tool (ftp://ftp.sgc.ox.ac.uk/pub/biophysics) and Graphpad Prism 5.0.0.228 (Graph Pad Software Inc.). A t-test was performed with Graphpad Prism to validate the significance of the results.

In Vitro Analytics

To analyse the products in vitro, 500 μL of 1 mg/mL CotB2 in Buffer B were incubated for 18 h at RT with 50 μg of GGDP or FDP. Subsequently the products were extracted using 3 times 200 μl analytical grade n-hexane. The 3 extractions were pooled and analysed using a Trace GC–MS Ultra system with DSQ II (Thermo Scientific, USA). 1 μl of the sample was injected with 1/10 split ratio by a TriPlus auto sampler onto a SGE BPX5 column (30 m, I.D. 0.25 mm, film 0.25 μm). Injector temperature was set to 280 °C. Helium was used as carrier gas with a flow rate of 0.8 ml/min. Initial oven temperature was set to 50 °C and held for 2 min. Temperature was increased at a rate of 10 °C min^{-1} to 320 °C which was held for additional 3 min. MS data was recorded at 70 eV (EI) in positive mode ranging between 50 and 650. High resolution mass spectra were recorded using an Agilent 7250 GC/Q-TOF system. 1 μl of the sample was injected with a 1/19 split ratio by a 7693 A ALS onto an

Agilent segmented column (30 m, I.D. 320 μm, film 0.25 μm and 3.2 m, I.D. 100 μm, film 0.1 μm). Injector temperature was set to 280 °C. Helium was used as carrier gas with a flow rate of 0.8 ml/min. Initial oven temperature was set to 50 °C and held for 2.5 min. Temperature was increased at a rate of 10 °C min^{-1} to 320 °C which was held for additional 3 min. High resolution MS/MS spectra were recorded at 15 eV in positive mode between 50 and 650. Targeted MS/MS spectra were recorded for masses m/z 204.18, 222.19 and 272.74 with a collision energy of 15.0 V.

EnzyDock Docking

The X-ray crystallographic structure of CotB2^{WT} was taken from the RCSB protein data bank (6GGI[11]) and the CotB2^{V80L} variants was taken from the present experimental study. The coordinates of the hydrogen atoms in the protein were determined using the HBUILD facility available in the CHARMM program.[20,21] The protonation states of ionizable residues were set based on analysis of the hydrogen bonding network and are suitable for physiological pH. The possible protonation states of His residues (protonated on N_ε, N_δ, or both) were determined in the same manner. The native protein and cofactors were described by the standard CHARMM36 force field.[22] The ligands force field parameters for the GGDP substrate were generated based on the work of van der Kamp *et al.*[23] and CGenFF.[24]

CotB2^{WT} and its variant CotB2^{V80L} exist in dimeric form. However, the active site for ligand docking is far from the dimeric interface and hence only one of the monomer units was considered for docking studies. 3 Mg^{2+} ions and a pyrophosphate moiety ($P_2O_7^{2-}$) were considered as cofactors for docking. The docking grid was calculated with a grid spacing of 0.25 Å and dimensions of 30×30×30 Å^3 centred at the centre of mass of the ligand bound to the binding pocket in CotB2^{WT}. 225 different ligand conformations were generated during docking, which was performed without any restraints. In practice, the initial linear allyl cation was docked into the active site and the covalent bond to the pyrophosphate moiety was formed during docking. All the docking results discussed here are performed using the CHARMM-based docking program EnzyDock.[25] Active site volumes were computed as described previously.[26] QM/MM calculations were performed using the CHARMM-Q-Chem interface,[27] and the QM region was treated using the HF3c method.[28]

Free MD-Simulation

The initial structures for CotB2^{WT} and CotB2^{V80L} were taken from PDB ID 6GGI and 8QWS, chain A. The ligand's initial structure was the published docked position.[12] Missing residues at the termini were filled based on previous work.[12] Protein hydrogen atoms were added using the CHARMM HBUILD facility.[20] CHARMM 36 m[22] and CGenFF force field parameters[24] were used, and the system was set up using the CHARMM program.[20] Periodic boundary conditions (PBC) with a water box of 80 Å^3 with NaCl ions to neutralize charge and mimic experimental conditions were used (44 Na^+ and 42 Cl^-). The system was minimized, heated, and equilibrated before production runs of 10 ns were performed as detailed elsewhere.[29] Each protein was simulated using three replicas from the heating phase. Minor differences in the protocol are: The restrained minimization of the protein consisted of 1680 ABNR steps and the cofactors and ligand were restrained as well. During heating and equilibration, the protein, cofactors, and ligand were restrained to their initial position with a force constant of 1.0 kcal mol^{-1} Å^{-2}, and these restraints were removed prior to the production phase MD. The PME maximum grid spacing was set to 1.0 Å. The MD simulations were performed using the NAMD program.[30] Trajectory analysis and plotting was performed using widely used python libraries: MatPlotLib (v3.4.3), MDAnalysis (v2.7.0),[31] NumPy (v1.26.2),[32] Pandas(v1.5.3), Seaborn (v0.12.2(. PyMOL (v3.0.3; v2.4.1) was used for visualization. Using MDAnalysis, the frames were re-aligned to the initial position and RMSD values were calculated (Figures S13–S14). For density water analysis the "density" functionality was used.

Acknowledgements

T.B. and M.R. gratefully acknowledge funding by the Werner Siemens foundation for establishing the field of Synthetic Biotechnology at the Technical University of Munich (TUM). The synchrotron MX data was collected at beamline P14 operated by EMBL Hamburg at the PETRA III storage ring (DESY, Hamburg, Germany). We would like to thank G. Bourenkov for the assistance in using the beamline. We acknowledge access to beamlines of the BESSY II storage ring (Berlin, Germany) *via* the Joint Berlin MX-Laboratory sponsored by the Helmholtz Zentrum Berlin für Materialien und Energie, the Freie Universität Berlin, the Humboldt-Universität zu Berlin, the Max-Delbrück-Centrum, the Leibniz-Institut für Molekulare Pharmakologie and Charité – Universitätsmedizin Berlin. We are grateful to M. Wahl for continuous encouragement and support. We acknowledge support of A. de Amorim and B. V. Draegert in protein production and crystallization. This work was supported by a grant from the German-Israeli Foundation for Scientific Research and Development (Grant I-1497-302.5/2019) (D.T.M., B.L., T.B.) C.P.O.H. was supported by a scholarship from the Hanns Seidel Foundation with funds from Federal Ministry of Education and Research Germany (BMBF). Open Access funding enabled and organized by Projekt DEAL.

Conflict of Interests

The authors declare no conflict of interest.

Data Availability Statement

The atomic coordinates have been deposited in the Protein Data Bank with the accession code 8QWS (CotB2^{V80L}·$Mg^{2+}{}_3$·AHD), and 8QWT (CotB2^{V80L}). Diffraction images are deposited at protein diffraction.org under [10.18430/M38QWS] (CotB2^{V80L}·$Mg^{2+}{}_3$·AHD), as well as [10.18430/M38QWT] (CotB2^{V80L}). Docking results, electrostatic maps, volume calculations, and CHARMM scripts are available at Zenodo [10.5281/zenodo.10984171].

Keywords: terpene synthase · protein structure · biocatalysis · green chemistry · computational chemistry · QM/MM calculations

[1] D. W. Christianson, *Chem. Rev.* **2006**, *106*, 3412–3442.

[2] D. W. Christianson, *Science* **2007**, *316*, 60–61.
[3] D. W. Christianson, *Curr. Opin. Chem. Biol.* **2008**, *12*, 141–150.
[4] J. N. Whitehead, N. G. H. Leferink, L. O. Johannissen, S. Hay, N. S. Scrutton, *ACS Catal.* **2023**, *13*, 12774–12802.
[5] J. S. Dickschat, *Nat. Prod. Rep.* **2016**, *33*, 87–110.
[6] S. Y. Kim, P. Zhao, M. Igarashi, R. Sawa, T. Tomita, M. Nishiyama, T. Kuzuyama, *Chem. Biol.* **2009**, *16*, 736–743.
[7] B. Xu, D. J. Tantillo, J. D. Rudolf, *Angew. Chem. Int. Ed. Engl.* **2021**, *60*, 23159–23163.
[8] B. Xu, Z. Li, T. A. Alsup, M. A. Ehrenberger, J. D. Rudolf, *ACS Catal.* **2021**, *11*, 5906–5915.
[9] R. Janke, C. Görner, M. Hirte, T. Brück, B. Loll, *Acta Crystallogr. D Biol. Crystallogr.* **2014**, *70*, 1528–1537.
[10] T. Tomita, S. Y. Kim, K. Teramoto, A. Meguro, T. Ozaki, A. Yoshida, Y. Motoyoshi, N. Mori, K. Ishigami, H. Watanabe, M. Nishiyama, T. Kuzuyama, *ACS Chem. Biol.* **2017**, *12*, 1621–1628.
[11] R. Driller, S. Janke, M. Fuchs, E. Warner, A. R. Mhashal, D. T. Major, M. Christmann, T. Bruck, B. Loll, *Nat. Commun.* **2018**, *9*, 3971.
[12] K. Raz, R. Driller, N. Dimos, M. Ringel, T. Bruck, B. Loll, D. T. Major, *J. Am. Chem. Soc.* **2020**, *142*, 21562–21574.
[13] K. Raz, R. Driller, T. Bruck, B. Loll, D. T. Major, *Beilstein J. Org. Chem.* **2020**, *16*, 50–59.
[14] J. Jumper, R. Evans, A. Pritzel, T. Green, M. Figurnov, O. Ronneberger, K. Tunyasuvunakool, R. Bates, A. Zidek, A. Potapenko, A. Bridgland, C. Meyer, S. A. A. Kohl, A. J. Ballard, A. Cowie, B. Romera-Paredes, S. Nikolov, R. Jain, J. Adler, T. Back, S. Petersen, D. Reiman, E. Clancy, M. Zielinski, M. Steinegger, M. Pacholska, T. Berghammer, S. Bodenstein, D. Silver, O. Vinyals, A. W. Senior, K. Kavukcuoglu, P. Kohli, D. Hassabis, *Nature* **2021**, *596*, 583–589.
[15] C. Görner, I. Hauslein, P. Schrepfer, W. Eisenreich, T. Brück, *Chemcatchem* **2013**, *5*, 3289–3298.
[16] W. Kabsch, *Acta Crystallogr. D Biol. Crystallogr.* **2010**, *66*, 125–132.
[17] A. J. McCoy, R. W. Grosse-Kunstleve, P. D. Adams, M. D. Winn, L. C. Storoni, R. J. Read, *J. Appl. Crystallogr.* **2007**, *40*, 658–674.
[18] P. D. Adams, P. V. Afonine, G. Bunkoczi, V. B. Chen, I. W. Davis, N. Echols, J. J. Headd, L. W. Hung, G. J. Kapral, R. W. Grosse-Kunstleve, A. J. McCoy, N. W. Moriarty, R. Oeffner, R. J. Read, D. C. Richardson, J. S. Richardson, T. C. Terwilliger, P. H. Zwart, *Acta Crystallogr. D Biol. Crystallogr.* **2010**, *66*, 213–221.
[19] A. Casanal, B. Lohkamp, P. Emsley, *Protein Sci.* **2020**, *29*, 1069–1078.
[20] B. R. Brooks, C. L. Brooks, A. D. MacKerell, L. Nilsson, R. J. Petrella, B. Roux, Y. Won, G. Archontis, C. Bartels, S. Boresch, A. Caflisch, L. Caves, Q. Cui, A. R. Dinner, M. Feig, S. Fischer, J. Gao, M. Hodoscek, W. Im, K. Kuczera, T. Lazaridis, J. Ma, V. Ovchinnikov, E. Paci, R. W. Pastor, C. B. Post, J. Z. Pu, M. Schaefer, B. Tidor, R. M. Venable, H. L. Woodcock, X. Wu, W. Yang, D. M. York, M. Karplus, *J. Comput. Chem.* **2009**, *30*, 1545–1614.
[21] B. R. Brooks, R. E. Bruccoleri, B. D. Olafson, D. J. States, S. Swaminathan, M. Karplus, *J Comput. Chem.* **1983**, *4*, 187–217.
[22] J. Huang, S. Rauscher, G. Nawrocki, T. Ran, M. Feig, B. L. D. Groot, H. Grubmüller, A. D. Mackerell, *Nat. Methods* **2017**, *14*, 71–73.
[23] M. W. van der Kamp, J. Sirirak, J. Zurek, R. K. Allemann, A. J. Mulholland, *Biochemistry* **2013**, *52*, 8094–8105.
[24] K. Vanommeslaeghe, E. Hatcher, C. Acharya, S. Kundu, S. Zhong, J. Shim, E. Darian, O. Guvench, P. Lopes, I. Vorobyov, A. D. Mackerell, *J. Comput. Chem.* **2010**, *31*, 671–690.
[25] S. Das, M. Shimshi, K. Raz, N. Nitoker Eliaz, A. R. Mhashal, T. Ansbacher, D. T. Major, *J. Chem. Theory Comput.* **2019**, *15*, 5116–5134.
[26] R. Schwartz, S. Zev, D. T. Major, *Angew. Chem. Int. Ed. Engl.* **2024**, e202400743.
[27] H. L. Woodcock, M. Hodoscek, A. T. B. Gilbert, P. M. W. Gill, H. F. Schaefer, B. R. Brooks, *J. Comput. Chem.* **2007**, *28*, 1485–1502.
[28] R. Sure, S. Grimme, *J. Comput. Chem.* **2013**, *34*, 1672–1685.
[29] R. Schwartz, S. Ruthstein, D. T. Major, *Protein Sci.* **2022**, *31*, e4464.
[30] J. C. Phillips, R. Braun, W. Wang, J. Gumbart, E. Tajkhorshid, E. Villa, C. Chipot, R. D. Skeel, L. Kale, K. Schulten, *J. Comput. Chem.* **2005**, *26*, 1781–1802.
[31] N. Michaud-Agrawal, E. J. Denning, T. B. Woolf, O. Beckstein, *J. Comput. Chem.* **2011**, *32*, 2319–2327.
[32] C. R. Harris, K. J. Millman, S. J. van der Walt, R. Gommers, P. Virtanen, D. Cournapeau, E. Wieser, J. Taylor, S. Berg, N. J. Smith, R. Kern, M. Picus, S. Hoyer, M. H. van Kerkwijk, M. Brett, A. Haldane, J. F. Del Rio, M. Wiebe, P. Peterson, P. Gerard-Marchant, K. Sheppard, T. Reddy, W. Weckesser, H. Abbasi, C. Gohlke, T. E. Oliphant, *Nature* **2020**, *585*, 357–362.

Manuscript received: April 17, 2024
Revised manuscript received: July 7, 2024
Accepted manuscript online: July 16, 2024
Version of record online: September 12, 2024